DINAME 2019 - Proceedings of the XVIII International Symposium on Dynamic Problems of Mechanics,
M.A. Savi, T.G. Ritto and W.M. Bessa (Editors), ABCM, Buzios, RJ, Brazil, March 10th to 15th, 2019

Closed-loop System Identification of an Unmanned Aerial System (UAS) with Flexible Wings using Subspace Methods

Raphaela Carvalho Machado Gonçalves Barbosa [1], **Luiz Carlos Sandoval Góes** [2], **Marcelo Santiago de Sousa** [3]

[1] Instituto Tecnológico de Aeronáutica, machado@ita.br

[2] Instituto Tecnológico de Aeronáutica, goes@ita.br

[3] Universidade Federal de Itajubá, marcelosousa.unifei@gmail.com

Abstract: This article presents a methodology for closed-loop system identification applied to an unmanned aerial system (UAS) with flexible wings using subspace methods. The investigated UAS is a small aircraft that has a total weight of 8.89 kg with a wing of area 0.8460 m^2 and span of 4 m. Its structural flexibility is a consequence of the composite material used to manufacture the wings besides the high aspect ratio about 18.91. Simulated data of a complete nonlinear rigid-body model coupled with two wing bending modes was developed and are used as input to the identification algorithm. The identification method is based on subspace techniques which applying algebra tools, e.g., singular value decomposition and orthogonal and oblique projections to solve the least-squares problem to determine the system matrices. In this work are used simulated data in order to validate the identification methodology presented and to obtain preliminary numerical results. The numerical results generated good models in state-space representation for the simulated aircraft, which may be evaluated to define the best control system strategy. A similar procedure is going to be performed later on experimental data collected from aircraft's flight-test campaigns.

Keywords: closed-loop system identification, subspace methods, flexible aircraft

INTRODUCTION

The system identification of aircrafts with flexible structures have been investigated [18], [19] mainly due to the problems caused by elastic effects in closed-loop flight control systems. In some cases the research for high aerodynamics efficiency causes a high-aspect-ratio resulting in a coupling of rigid and flexible dynamics.

A study about the influence of aircraft loads is presented in [14] in order to motivate the developing of accuracy models for aircrafts designed from new structural concepts. Thus, dynamic models of aircrafts containing the rigid-body derivatives and elastic-mode derivatives are needed to dynamic system analysis as well as to closed-loop control system design based on an accuracy model [1].

In the last years, techniques to estimate the aerodynamics coefficients have been applied and may be obtained, for example, from wind-tunnel tests while others may be estimated via numerical techniques. In both cases, efforts are needed to determine aerodynamic coefficients with confidence [3], [6].

On the other hand, approaches based on subspace methods [5] have been applied to obtain representative models. In particular, these models are referred to as black-box models since they not reflect the knowledge about the structure of the system. However, they offer an advantageous that are not an optimization algorithm and do not suffer from the inconveniences encountered in applying other techniques as the OEM method [12]. Thus, SIM methods are an efficient alternative for system identification.

Current researches about system identification have been performed with systems in closed-loop operation [10], [11], because in many situations an open-loop system have be avoid due to stability issues, as well as, to guarantee some performance requirements. In general, the system identification problem seeks to estimate an open-loop model from closed-loop system data [13].

In cases where the closed-loop operation is necessary, some classical methods, e.g., the prediction error method (PEM) and the output error method (OEM), may be fail and produce biased estimates. Thus, another class of identification algorithms based on subspace theory have been applied, just to deals with some difficulties that the feedback loop provides [9]. In this way, this work is addressed an procedure to identify parametric models for an unnamed aerial vehicle (UAV) with flexible wings under closed-loop conditions.

THE CASE STUDY: AN UNMANNED AERIAL SYSTEM WITH FLEXIBLE WINGS

This section describes the aircraft design performed by FT Systems in 2018 that is available at Aeronautical Systems Laboratory at Institute. Indeed, it is presented preliminary results obtained from experimental data and from simulated data using a previous model, both used to validate the proposed identification methodology that will be applied to flight-

test data collected from flight-test campaigns.

The Aircraft Design

As modern aircraft designers focus on increased aerodynamic efficiency and low structural weight is growing for the aircraft design a high aspect ratio combined with the lightweight composite structure. In this way, this article analyses an unmanned aerial system (UAS) designed with flexible wings just to evaluated the influence of the modes during its flight.

The Fig.1 shows the small aircraft with flexible wings. The UAS has a total weigh of 8.89 kg and span of 4 m with a wing of area 0.8460 m^2 resulting in an aspect ratio of $AR = 18.91$. The Selig S2091 profile describes an airfoil with high lifting and this profile will be used to estimate the aerodynamic coefficients using the strip theory.

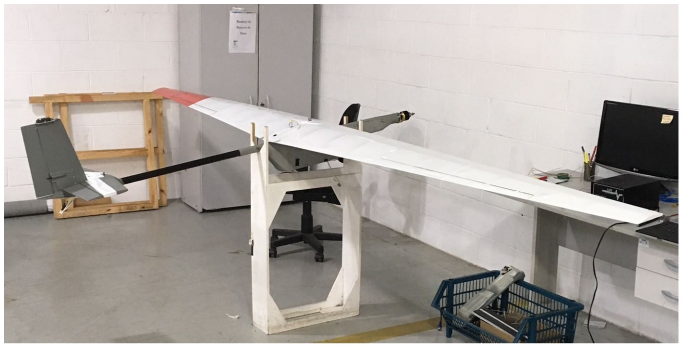

Mechanical characteristics.

Reference geometry	Total mass	Inertias
S=0.846 m^2	m=8.89 kg	I_{xx}=0.6835 kg.m^2
$\bar{c}$=0.2311 m		I_{yy}=0.978 kg.m^2
b=4 m		I_{zz}=1.607 kg.m^2
		I_{xz}=-0.05042 kg.m^2

Figure 1 – UAS with flexible wings designed and manufactured by FT systems in 2018 and mechanical characteristics.

The UAS has three control-surfaces deflections, an aileron, a rudder and an elevator and the propulsion thrust acts along the vehicle's fuselage, in X-axis. The propulsion thrust is considered a force that does not generate moment. The aircraft mechanical parameters, including the geometry, mass and other properties used in the simulation are summarized in Fig.1. The parameters in Fig.1 corresponding to initial values for the aircraft with rigid wings. Later, an estimate of the inertia properties for the flexible UAS should be made.

Experimental Modal Analysis for Characterization of the Wing Bending Modes

This work proposes, besides the identification of the aircraft, to determine the natural frequencies and mode shapes of the flexible wings based on the theory about the experimental modal analysis present in [8]. Preliminary results were obtained using only system output response due to limitations on performing the experiment using shakers.

A free vibration test was performed and the time histories of the accelerometers was collected just to evaluated the flexible structure. Further work is suggested to excite the structure with uncorrelated pseudo-random input using a shaker in order to estimate the generalized mass.

Some preliminary results were obtained using only the accelerometers response embedded in the wing of the UAS as depicted in Fig.2(a). The idea concerns in applying the Fast Fourier Transform (FFT) algorithm on collected experimental data from a free vibration test and to obtain the frequency of the structural modes. The methodology is the same as to draft the three quantities of the Frequency Response Function (FRF), but now only the Fourier Transform of the output is evaluated.

The FFT transforms the time domain data into the frequency domain. This is normally carried out using sampled time domain data and a simple Euler approximation of the finite Fourier integral called as Discrete Fourier Transform. In this work it was used the function `fft` implemented in MATLAB and the Fig.2(b) shows the FFT of the accelerometers data.

Preliminary results obtained from a Ground Vibration Test (GVT) with only the output measurements indicate the existence of at least four flexible modes, according to FFT of the data. Among other modes, the first two wing bending modes was identified. The first symmetric wing bending mode is about 4.85 Hz and the second anti-symmetric wing bending is about 12.37 Hz as summarized in Fig.2. In further work, at least these two lowest-frequency symmetric and anti-symmetric vibration modes will be integrated in the aircraft model in order to provide an accuracy and realistic simulated model of the studied flexible aircraft.

These preliminary results indicate that the first two frequencies are bending modes and an experimental data from a GVT test with input-output measurements is recommended in order to perform a complete experimental modal analysis. More informative data may be acquired from a GVT using, for example, a shaker to excite the system. It is desired to obtain more information about the third and four modes besides the generalized mass.

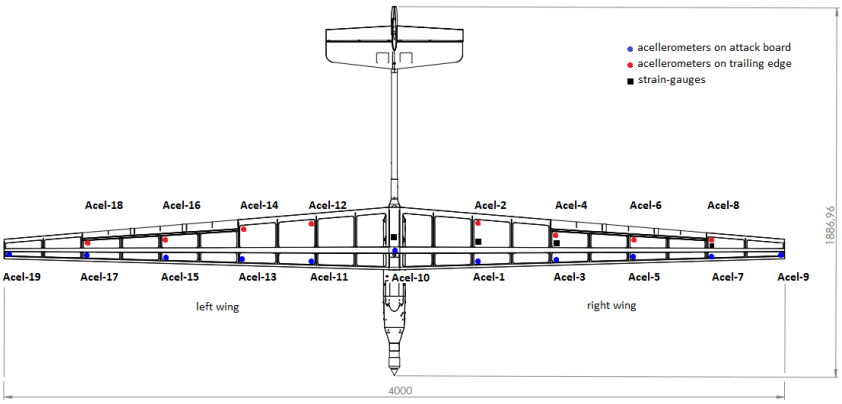

Modal frequencies.

Order	Mode	Natural frequency (Hz)
1	1 st wing symmetric bending	4.85
2	2 nd wing anti-symmetric bending	12.37
3	not determined	15.59
4	not determined	19.76

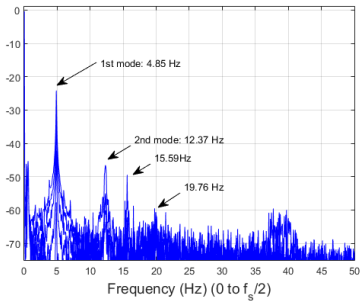

Figure 2 – (a) Distribution of accelerometers and strain gauges on the aircraft structure and (b) The Fast Fourier Transform from experimental data and the modal frequencies.

The Equations of Motion for Modeling of the UAS

Many aircrafts are well approximated as rigid bodies with gravitational, aerodynamics and propulsive forces acting on them. Their motions may then be described by giving the position and velocity of a set of body-fixed axes with respect to a orientation and angular velocity of a set of body-fixed with respect to a set of reference axes.

For modeling the forces and moments on the aircraft (in this work aircraft=vehicle), the earth-fixed reference axes may be approximated as inertial axes and the dynamic equations of motion that govern the rigid-body translation motion of the aircraft are [20]

$$m(\dot{u} - vr + wq) = -mg\sin\theta + F_{A_x} + F_{P_X} \quad (1)$$

$$m(\dot{v} + ur - wp) = mg\cos\theta\sin\phi + F_{A_y} + F_{P_y} \quad (2)$$

$$m(\dot{w} - uq + vp) = mg\cos\theta\cos\phi + F_{A_z} + F_{P_z} \quad (3)$$

where the two components on the right-hand sides the aerodynamic and propulsive forces.

In the same way, the equations of motion for the rigid-body rotational motion of the aircraft that include the aerodynamic and propulsive moment effects are given by

$$I_{xx}\dot{p} - (I_{yy} - I_{zz})qr - I_{xy}(\dot{q} - pr) - I_{yz}(q^2 - r^2) - I_{xz}(\dot{r} + pq) = L_A + L_P \quad (4)$$

$$I_{yy}\dot{q} - (I_{xx} - I_{zz})pr - I_{xy}(\dot{p} + qr) - I_{yz}(\dot{r} - pq) + I_{xz}(p^2 - r^2) = M_A + M_P \quad (5)$$

$$I_{zz}\dot{r} - (I_{yy} - I_{xx})pq + I_{xy}(q^2 - p^2) - I_{yz}(\dot{q} + pr) - I_{xz}(\dot{p} - qr) = N_A + N_P \quad (6)$$

These equations contains the rigid-body variables for an aircraft and the elastic effects will enter in the above equations through changes in the forces and moments on the right-hand side [17].

In this present investigation, an previous analytical rigid-body nonlinear model coupled with only two symmetric wing bending modes is presented and simulated to generate synthetic data. The previous model for the flexible aircraft is performed assuming the expression of the force coefficients in the wing axes in the following form

$$C_D = C_{D_0} + \frac{C_L^2}{\pi eAR} \quad (7)$$

$$C_Y = C_{Y_0} + C_{Y_\beta}\beta + C_{Y_p}\frac{b}{2V}p + C_{Y_r}\frac{b}{2V}r + C_{Y_{\delta_a}}\delta_a + C_{Y_{\delta_r}}\delta_r \quad (8)$$

$$C_L = C_{L_0} + C_{L_\alpha}\alpha + C_{L_q}\frac{\bar{c}}{2V}q + C_{L_{\delta_e}}\delta_e + \underbrace{C_{L_{\eta_1}}\eta_1 + C_{L_{\dot{\eta}_1}}\frac{\bar{c}}{2V}\dot{\eta}_1 + C_{L_{\eta_2}}\eta_2 + C_{L_{\dot{\eta}_2}}\frac{\bar{c}}{2V}\dot{\eta}_2}_{\text{Effects of modal displacement and velocity}} \quad (9)$$

and the moment coefficients expressed as

$$C_l = C_{l_0} + C_{l_\beta}\beta + C_{l_p}\frac{b}{2V}p + C_{l_r}\frac{b}{2V}r + C_{l_{\delta_a}}\delta_a + C_{l_{\delta_r}}\delta_r \tag{10}$$

$$C_m = C_{m_0} + C_{m_\alpha}\alpha + C_{m_q}\frac{\bar{c}}{2V}q + C_{m_{\delta_e}}\delta_e + \underbrace{C_{m_{\eta_1}}\eta_1 + C_{m_{\dot{\eta}_1}}\frac{\bar{c}}{2V}\dot{\eta}_1 + C_{m_{\eta_2}}\eta_2 + C_{m_{\dot{\eta}_2}}\frac{\bar{c}}{2V}\dot{\eta}_2}_{\text{Effects of modal displacement and velocity}} \tag{11}$$

$$C_n = C_{n_0} + C_{n_\beta}\beta + C_{n_p}\frac{b}{2V}p + C_{n_r}\frac{b}{2V}r + C_{n_{\delta_a}}\delta_a + C_{n_{\delta_r}}\delta_r \tag{12}$$

The generalized force coefficients are modeling as Eq.13 and Eq.14.

$$Q_1 = \underbrace{C_{Q_{1\alpha}}\alpha + C_{Q_{1q}}\frac{\bar{c}}{2V}q}_{\text{Rigid-body}} + \underbrace{C_{Q_{1\eta_1}}\eta_1 + C_{Q_{1\dot{\eta}_1}}\frac{\bar{c}}{2V}\dot{\eta}_1 + C_{Q_{1\eta_2}}\eta_2 + C_{Q_{1\dot{\eta}_2}}\frac{\bar{c}}{2V}\dot{\eta}_2}_{\text{Elastic effects}} \tag{13}$$

$$Q_2 = \underbrace{C_{Q_{2\alpha}}\alpha + C_{Q_{2q}}\frac{\bar{c}}{2V}q}_{\text{Rigid-body}} + \underbrace{C_{Q_{2\eta_1}}\eta_1 + C_{Q_{2\dot{\eta}_1}}\frac{\bar{c}}{2V}\dot{\eta}_1 + C_{Q_{2\eta_2}}\eta_2 + C_{Q_{2\dot{\eta}_2}}\frac{\bar{c}}{2V}\dot{\eta}_2}_{\text{Elastic effects}} \tag{14}$$

A preliminary estimative of the stability and control derivatives used in this work, just to generate synthetic data, are summarized in Tab.1 and were obtained from an initial design of the aircraft with rigid wings about at velocity of 12.95 m/s.

Only to provide synthetic closed-loop data was included only two elastic effects on longitudinal motion equations. The flexible effects were included based on parameters from literature with some adjustments. Later, as already mentioned, is needed to provide a more realistic model based on experimental modal analysis and other techniques.

Table 1 – Longitudinal and lateral-directional nondimensional derivatives.

C_{D0}	0.017	C_{Y0}	0	C_{L0}	0.55	C_{l0}	0	C_{m0}	0.023	C_{n0}	0
		$C_{Y\beta}$	-0.2989	$C_{L\alpha}$	5.2	$C_{l\beta}$	-0.04	$C_{m\alpha}$	-1	$C_{n\beta}$	0.1078
		C_{Yp}	-0.0634	C_{Lq}	8	C_{lp}	-0.5608	C_{mq}	-18.55	C_{np}	-0.1248
		C_{Yr}	0.2742	$C_{L\delta_e}$	0.55	C_{lr}	0.1881	$C_{m\delta_e}$	-1.89	C_{nr}	-0.0945
		$C_{Y\delta_a}$	0			$C_{l\delta_a}$	0.089			$C_{n\delta_a}$	0
		$C_{Y\delta_r}$	0			$C_{l\delta_r}$	-0.0052			$C_{n\delta_r}$	0.0333

A flight-test condition

In order to evaluate with more consistency the preliminary numerical results for flight vehicle system identification, this results are best described by an example. Thus, a case study was performed considering a simple reference flight condition, a straight and level cruise, in order to provide the decoupling between the longitudinal and lateral-directional dynamics becoming more easy to validate the identification methodology presented.

In stead rectilinear flight $\dot{u} = \dot{v} = \dot{w} = \dot{p} = \dot{q} = \dot{r} = 0$ and usually the wings are level, $\phi = 0$ [4]. Thus, an equilibrium condition for the aircraft in a straight and level cruise can be obtained by

$$\dot{X} = 0 \tag{15}$$

where $X^{n\times 1}$ is the state vector. The Eq.15 is the equation of equilibrium solved numerically using the function `fsolve` implemented in MATLAB.

An equilibrium "trim" condition was obtained resulting in trimmed values for the state, control surface deflections and propulsion. The nonlinear numerical model was linearized about the equilibrium ("trim") condition of straight and level cruise at an altitude of 304.8 m and at a velocity of 12.95 m/s. In this point of analysis, it is possible to note that the equations, nonlinear and linear, decouple for reference flight condition involving, in this case, zero reference bank and sideslip angles.

The goal of the linearized matrices is to determine eigenvalues of the linearized dynamics (or to solve the characteristic equation of this system) and to distinguish between longitudinal and lateral-directional motions. Also, control system design may be performed based on these matrices.

The Fig.3 summarizes the eigenvalues to the linear model containing the longitudinal rigid-body modes (the phugoid and short-period modes) and lateral-directional rigid-body modes (the roll, spiral and dutch roll modes), indeed the two

flexible wing modes. A way to present the eigenvalues is plotting the real part versus the imaginary part according to Fig.3.

Natural frequency w_n and damping factor ζ for eigenvalues.

eigenvalues	w_n	ζ	mode
$-4.01 \pm j4.90$	6.34	0.63	short period
$-0.0042 \pm j0.84$	0.84	0.005	phugoid
0	-	-	due altitude
-58.88	-	1	roll
0.25	-	-1	spiral
$-3.28 \pm j4.95$	5.94	0.55	dutch roll
$-1.07 \pm j30.45$	30.47	0.035	1st wing symmetric bending
$-1.71 \pm j77.67$	77.69	0.022	2nd wing symmetric bending

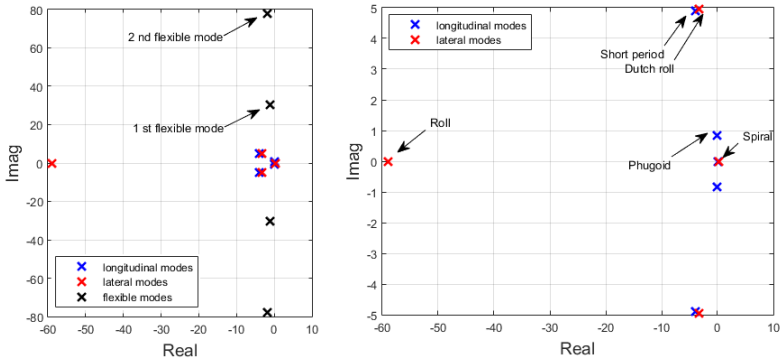

Figure 3 – Eigenvalues of the linearized dynamics.

Note that the longitudinal mode has the biggest frequency about 6.61 rad/s while the flexible mode is about 30.47 rad/s. Therefore, it indicates a priori, that there is not a significant coupling between the rigid and flexible dynamics, but the effects of the structural deformations need to be evaluated.

DATA GATHERING FOR CLOSED-LOOP SYSTEM IDENTIFICATION

The real flight test data are not available yet. Thus, simulated flight data was generated for a flexible aircraft considering the nonlinear analytical model previously presented. A flight condition of a straight and level cruise was considered to perform the system identification of the longitudinal dynamic model about an equilibrium point.

The block diagram of an attitude hold autopilot is shown in Fig.4 just because the feedback structure is normally used when the aircraft is in wings-level flight. The controlled variable is the attitude angle θ and the sensor is an attitude reference gyro. The sample time used in all simulations to generate synthetic data is 10 ms that corresponding to 100 Hz.

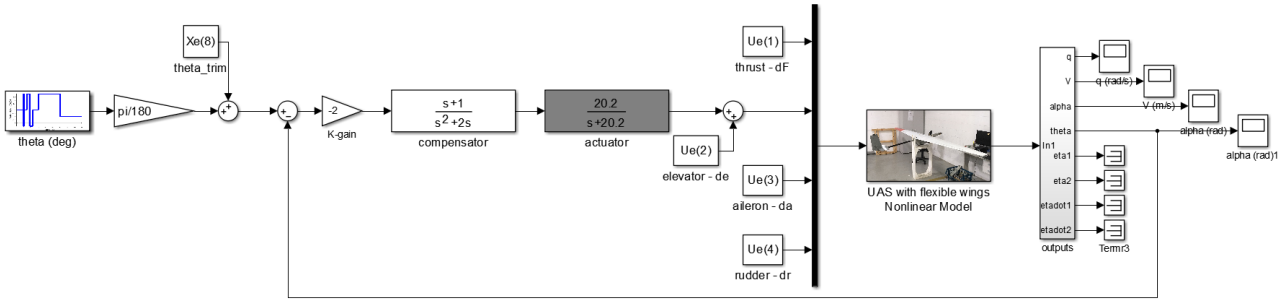

Figure 4 – An attitude hold implemented in MATLAB/SIMULINK.

The control design involves a theta-loop root-locus design which is used to provide the gain of the controller. As the open-loop transfer function does not have a integrator, it was inserted PI controller. This design has the advantage that a small value for K_θ is necessary to reduce the steady-state error.

The time histories of the system input (the control signal) and the attitude-hold response for a reference signal are used for subspace system identification. Of all available output responses, four output signals related to rigid-body states are used, q, V, α and θ indeed the generalized velocities and displacements η_1, $\dot{\eta}_1$, η_2 and $\dot{\eta}_2$. The input signal is the elevator deflection δ_e. The reference signal is only used to excite the system dynamics.

THE CLOSED-LOOP SYSTEM IDENTIFICATION

In many closed-loop systems the usual identification procedure may be fail and produce biasing estimates due to the correlation between the input signal and the noise. In this way, an alternative just to deals with closed-loop system data is applying the subspace techniques. Among others problems, lower representative models mean that the closed-loop system data are not informative.

Assuming that the data are informative and the problem with the closed-loop data is only the correlation between

the input signal and the noise depending of the feedback loop, in this section is presented the mathematical formulation the DSR (combined deterministic and stochastic system identification and realization) algorithm proposed by [7] for parametric identification of the UAS with flexible wings.

The Mathematical Formulation

Consider a discrete-time stochastic linear system

$$\begin{aligned} x_{k+1} &= \mathbf{A}x_k + \mathbf{B}u_k + w_k \\ y_k &= \mathbf{C}x_k + \mathbf{D}u_k + v_k \end{aligned} \tag{16}$$

where u_k is the input vector, y_k is the output vector, $\mathbf{A} \in \mathbb{R}^{n\times n}$, $\mathbf{B} \in \mathbb{R}^{n\times m}$, $\mathbf{C} \in \mathbb{R}^{l\times n}$and $\mathbf{D} \in \mathbb{R}^{l\times m}$ are the system matrices. w_k and v_k are Gaussian white noise vectors with zero mean and covariance matrices,

$$E\left\{ \begin{bmatrix} w_p \\ v_p \end{bmatrix} \begin{bmatrix} w_q^T & v_q^T \end{bmatrix} \right\} = \begin{bmatrix} Q & S \\ S^T & R \end{bmatrix} \delta_{pq} \tag{17}$$

It is possible to derive a filtering algorithm for Eq.16 that produces the one-step predicted estimates $\hat{x}_k$ and $\hat{x}_{k+1}$ using another form to write this equation [13]. Thus, the system dynamic may be described by a innovation model

$$\begin{aligned} x_{k+1} &= \mathbf{A}x_k + \mathbf{B}u_k + \mathbf{K}\varepsilon_k \\ y_k &= \mathbf{C}x_k + \mathbf{D}u_k + \varepsilon_k \end{aligned} \tag{18}$$

where ε_k is the innovation process.

From Eq.18 is possible yields the Kalman filter prediction model,

$$\begin{aligned} x_{k+1} &= (\mathbf{A} - \mathbf{KC})x_k + (\mathbf{B} - \mathbf{KD})u_k + \mathbf{K}y_k \\ y_k &= \mathbf{C}x_k + \mathbf{D}u_k + \varepsilon_k \end{aligned} \tag{19}$$

with

$$\mathbf{K} = (\mathbf{APC}^T + \mathbf{S})(\mathbf{CPC}^T + \mathbf{R})^{-1} \tag{20}$$

The matrix $\mathbf{K} \in \mathbb{R}^{n\times l}$ is the stationary Kalman filter gain when N is sufficiently large, $\varepsilon_k \in \mathbb{R}^{n\times l}$ is a Gaussian white noise, known as innovation process, and $\mathbf{P} > 0$ is a positive symmetric matrix give by Riccati's equation

$$\mathbf{P} = \mathbf{APA}^T - (\mathbf{APC}^T + \mathbf{S})(\mathbf{CPC}^T + \mathbf{R})^{-1}(\mathbf{APC}^T + \mathbf{S})^T + \mathbf{Q} \tag{21}$$

Many subspace methods, including the DSR algorithm, work with this model. The mathematical formulation presented in this section is based on Eq.19 and considering this representation, the estimation error is independent of the Kalman filter state vectors, otherwise, the minimum variance estimate is unbiased. This is a consequence of the optimality of the Kalman filter $\hat{x}(t+m/t)$ that is given when the estimation error $\tilde{x}(t+m/t)$ is orthogonal to the data space.

In general, the SIM methods are different in what the linear algebra tools may be used to obtain the data projections. The state estimates are constructed from given input-output data and the state space model is obtained by solving a least-squares problem.

There are algorithms that use the state vector, e.g. the N4SID method or use the extended observability matrix, e.g. the MOESP method to obtain the system matrices. It is demonstrated that the DSR algorithm uses the state vector to compute the system matrices.

In formulation of the subspace identification problem, it is necessary to define an extended state-space model just to generate the data space formed by block Hankel matrices of the input and output data.

The state vector and output vector in the matrix form is given by

$$\begin{aligned} \mathbf{X}_{J/1} &= \begin{bmatrix} \widetilde{\mathbf{C}}_J^d & \widetilde{\mathbf{C}}_J^s \end{bmatrix} \begin{bmatrix} \mathbf{U}_{0/J} \\ \mathbf{Y}_{0/J} \end{bmatrix} + (\mathbf{A} - \mathbf{KD})^J \mathbf{X}_{0/1} \\ \mathbf{Y}_{J/L} &= \widetilde{\mathbf{O}}_L \mathbf{X}_{J/1} + \widetilde{\mathbf{H}}_L^d \mathbf{U}_{J/L} + \widetilde{\mathbf{H}}_L^s \varepsilon_{J/L} \end{aligned} \tag{22}$$

where J and L are, respectively, the past and future horizons of the block Hankel matrices of the input and/or output data.

The future states are defined as $\mathbf{X}_{J/1} = \begin{bmatrix} x_J & x_{J+1} & \dots & x_{N-J+L} \end{bmatrix}$ and $\tilde{C}_J^d$ and $\tilde{C}_J^s$, are the reversed extended controllability matrix.

The reversed extended controllability matrix of the pair $(\mathbf{A} - \mathbf{KC}, \mathbf{B} - \mathbf{KD})$ is

$$\tilde{C}_J^d = \begin{bmatrix} \mathbf{A}^{i-1}\mathbf{B} & \mathbf{A}^{i-2}\mathbf{B} & \dots & \mathbf{B} \end{bmatrix} \tag{23}$$

and the reversed extended controllability matrix of the pair $(\mathbf{A}-\mathbf{KC},\mathbf{K})$ is

$$\tilde{C}_J^s = \begin{bmatrix}\mathbf{A}^{i-1}\mathbf{C} & \mathbf{A}^{i-2}\mathbf{C} & \ldots & \mathbf{C}\end{bmatrix} \tag{24}$$

The block Hankel matrix is used in the formulation of extended state space model. For construction of this matrix, consider a given measurement sequence,

$$\mathbf{s}_k = \begin{bmatrix}\mathbf{s}_0 & \mathbf{s}_1 & \mathbf{s}_2 & \ldots & \mathbf{s}_{N-1}\end{bmatrix} \in \mathbb{R}^{nr\times N} \tag{25}$$

where nr e N are, respectively, the quantity of system input and/or the output and the sample number. The block Hankel matrix is defined as

$$\mathbf{S}_{j/i} = \begin{bmatrix} \mathbf{s}_j & \mathbf{s}_{j+1} & \mathbf{s}_{j+2} & \cdots & \mathbf{s}_{j+nc-1} \\ \mathbf{s}_{j+1} & \mathbf{s}_{j+2} & \mathbf{s}_{j+3} & \cdots & \mathbf{s}_{j+nc} \\ \cdots & \cdots & \cdots & \cdots & \cdots \\ \mathbf{s}_{j+i-1} & \mathbf{s}_{j+i} & \mathbf{s}_{j+i+1} & \cdots & \mathbf{s}_{j+i+nc-2} \end{bmatrix} \in \mathbb{R}^{inr\times N} \tag{26}$$

where i is the order of the block Hankel matrix and j is the index of the first matrix element. Based on the experimental data sequence, $nc = N-j-i+1$ is the number of columns in the Hankel matrix.

The innovation process is obtained directly from experimental data projection. This procedure consists in splitting the deterministic signal of the residue. In open-loop, the **D** matrix may be non-null and should be identified.

Considering the closed-loop problem, a deterministic component of output signal is given by a orthogonal projection of the experimental data,

$$\mathbf{y}_{J/1}^d = \mathbf{Y}_{J/1} / \begin{bmatrix}\mathbf{U}_{0/J} \\ \mathbf{Y}_{0/J}\end{bmatrix} \tag{27}$$

and the innovation sequence is estimated by

$$\varepsilon_{J/1} = \mathbf{Y}_{J/1} - \mathbf{Y}_{J/1} / \begin{bmatrix}\mathbf{U}_{0/J} \\ \mathbf{Y}_{0/J}\end{bmatrix} \tag{28}$$

Thus, firstly the algorithm split the output data into a signal part and a noise part as pointed out,

$$\mathbf{y}_{J/1} = \mathbf{y}_{J/1}^d + \varepsilon_{J/1} \tag{29}$$

After removing the effect of noise on input data, the system matrices are calculated by solving a deterministic identification problem with matrix **D** null.

$$\begin{aligned} \mathbf{x}_{k+1} &= \mathbf{A}\mathbf{x}_k + \begin{bmatrix}\mathbf{B} & \mathbf{K}\end{bmatrix}\begin{bmatrix}\mathbf{u}_k \\ \varepsilon_k\end{bmatrix} \\ \mathbf{y}_k^d &= \mathbf{C}\mathbf{x}_k \end{aligned} \tag{30}$$

In this step, a new input and output data is defined as follows

$$\begin{aligned} \mathbf{u}_k : &= \begin{bmatrix}\mathbf{U}_{J/1} \\ \varepsilon_{J/1}\end{bmatrix} \\ \mathbf{y}_k : &= \mathbf{y}_{J/1}^d \end{aligned} \tag{31}$$

where $k = J, J+1, J+2, ..., N-1$ and $N := N-J$ is the sample number.

It is used the N4SID proposed by [13] to solve the deterministic identification problem, in which the first step consists in to obtain an oblique projection of future output onto past output-input along of future inputs applying a LQ decomposition.

$$\begin{bmatrix}\mathbf{U}_{L/L} \\ \mathbf{U}_{0/L} \\ \mathbf{Y}_{0/L} \\ \mathbf{Y}_{L/L}\end{bmatrix} = \begin{bmatrix}\mathbf{L}_{11} & 0 & 0 & 0 \\ \mathbf{L}_{21} & \mathbf{L}_{22} & 0 & 0 \\ \mathbf{L}_{31} & \mathbf{L}_{32} & \mathbf{L}_{33} & 0 \\ \mathbf{L}_{41} & \mathbf{L}_{42} & \mathbf{L}_{43} & \mathbf{L}_{44}\end{bmatrix}\begin{bmatrix}\mathbf{Q}_1^T \\ \mathbf{Q}_2^T \\ \mathbf{Q}_3^T \\ \mathbf{Q}_4^T\end{bmatrix} \tag{32}$$

Rearranging the Eq.32,

$$\begin{bmatrix}\mathbf{U}_{L/L} \\ \begin{bmatrix}\mathbf{U}_{0/L} \\ \mathbf{Y}_{0/L}\end{bmatrix} \\ \mathbf{Y}_{L/L}\end{bmatrix} = \begin{bmatrix}\mathbf{R}_{11} & 0 & 0 \\ \mathbf{R}_{21} & \mathbf{R}_{22} & 0 \\ \mathbf{R}_{31} & \mathbf{R}_{32} & 0\end{bmatrix}\begin{bmatrix}\overline{\mathbf{Q}}_1^T \\ \overline{\mathbf{Q}}_2^T \\ \overline{\mathbf{Q}}_3^T\end{bmatrix} \tag{33}$$

where

$$\mathbf{R}_{11} = \begin{bmatrix}\mathbf{L}_{11}\end{bmatrix}, \mathbf{R}_{21} = \begin{bmatrix}\mathbf{L}_{21} \\ \mathbf{L}_{31}\end{bmatrix}, \mathbf{R}_{22} = \begin{bmatrix}\mathbf{L}_{22} & 0 \\ \mathbf{L}_{32} & L_{33}\end{bmatrix}, \mathbf{R}_{31} = \begin{bmatrix}\mathbf{L}_{41}\end{bmatrix}, \mathbf{R}_{32} = \begin{bmatrix}\mathbf{L}_{42} & \mathbf{L}_{43}\end{bmatrix}$$

$$\overline{\mathbf{Q}}_1^T = \begin{bmatrix}\mathbf{Q}_1^T\end{bmatrix}, \overline{\mathbf{Q}}_2^T = \begin{bmatrix}\mathbf{Q}_2^T \\ \mathbf{Q}_3^T\end{bmatrix}, \overline{\mathbf{Q}}_3^T = \begin{bmatrix}\mathbf{Q}_4^T\end{bmatrix}$$

From Eq.33, the output equation of future data is given by

$$\mathbf{Y}_{L/L} = \mathbf{R}_{31}\overline{\mathbf{Q}}_1^T + \mathbf{R}_{32}\overline{\mathbf{Q}}_2^T \tag{34}$$

Substituting the terms of $\overline{\mathbf{Q}}_1^T$ and $\overline{\mathbf{Q}}_2^T$ into Eq.34), from Eq.33, yields

$$\mathbf{Y}_{L/L} = \underbrace{\mathbf{R}_{32}\mathbf{R}_{22}^{\dagger}\begin{bmatrix}\mathbf{U}_{0/L} \\ \mathbf{Y}_{0/L}\end{bmatrix}}_{\widetilde{\mathbf{O}}_L\mathbf{X}_{L/1}} + \underbrace{\left(\mathbf{R}_{31} - \mathbf{R}_{32}\mathbf{R}_{22}^{\dagger}\mathbf{R}_{21}\right)\mathbf{R}_{11}^{-1}\mathbf{U}_{L/L}}_{\widetilde{\mathbf{H}}_L^d\mathbf{U}_{J/L}} \tag{35}$$

where the Eq.35 is similar to Eq.22 of output and, for comparison, the projection equation is given by

$$\widetilde{\mathbf{O}}_L\mathbf{X}_{L/1} = \mathbf{R}_{32}\mathbf{R}_{22}^{\dagger}\begin{bmatrix}\mathbf{U}_{0/L} \\ \mathbf{Y}_{0/L}\end{bmatrix} \tag{36}$$

Applying a singular value decomposition in the projection matrix

$$\mathbf{R}_{32}\mathbf{R}_{22}^{\dagger}\begin{bmatrix}\mathbf{U}_{0/L} \\ \mathbf{Y}_{0/L}\end{bmatrix} = \mathbf{U}\mathbf{S}\mathbf{V}^T \approx \mathbf{U}_1\mathbf{S}_1\mathbf{V}_1^T \tag{37}$$

The observability matrix is given by

$$\widetilde{\mathbf{O}}_L = \mathbf{U}_1\mathbf{S}_1^{\frac{1}{2}} \tag{38}$$

with

$$\mathbf{C} = \widetilde{\mathbf{O}}_L(1:l, 1:n) \tag{39}$$

and an estimated state sequence of the system is

$$\widetilde{\mathbf{X}}_{J/1} = \mathbf{S}_1^{\frac{1}{2}}\mathbf{V}_1^T \tag{40}$$

Thus, from the input-output data and estimated state sequence, it is possible to solve the least-squares problem from Eq.30 to determine the system matrices **A** and **B** and the filter Kalman gain **K**. Moreover, an estimate of residue covariance matrix may be calculated by [2]

$$\mathbf{P}_{\varepsilon} = \frac{1}{nc}\boldsymbol{\varepsilon}_{J/1}\boldsymbol{\varepsilon}_{J/1}^T \tag{41}$$

with *nc* defined according to Eq.26.

Results from identification

In order to investigate the performance of the DSR algorithm, developed by [7] to identify the system dynamics even the closed-loop data corrupted by measurements noise, it was added in each longitudinal variables, q, α and θ, Gaussian white-noises with suitable Signal-to-Noise Ratio (SNR). The time histories of the system input (the control signal) and the attitude-hold response for a reference signal is depicted in Fig.5. The closed-loop system data are used for subspace system identification.

Applying the DSR algorithm to closed-loop system data, a singular value decomposition was obtained with identification parameters J=140 and L=2 that corresponding at past and future horizons, respectively. The order n=9 was adopted for the linear model, previously based on the analytical model and according to the most representative singular values displayed.

As most of the output predictions calculated from the identified model exhibited a unstable behavior, along of this work only the Bode plots are depicted. Thus, the linear identified model obtained from closed-loop data corrupted by measurements noise is shown in Fig.6.

Note that even in presence of the measurements noise, the DSR algorithm captures unbiased estimatives and into the frequencies range that the system was excited the model is representative because in this case there is a good fit between the Bode plots of the system and the identified model.

Although the partial derivatives with respect to the motion variables and control inputs dot not appear explicit in the model, there is the modern control system design that is based only on state-space models. Thus, the subspace approach is an alternative to identify a representative model for the aircrafts in closed-loop operation.

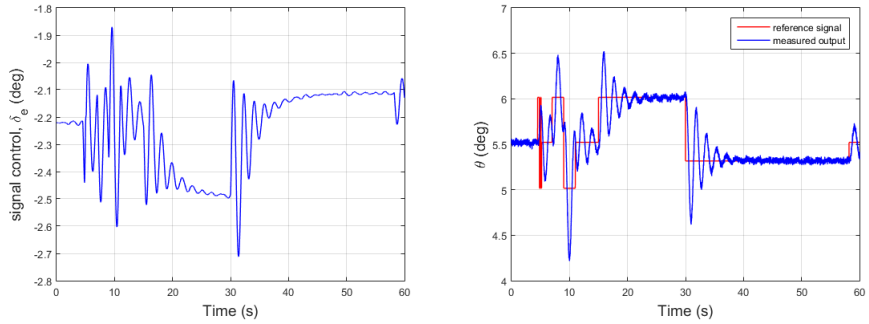

Figure 5 – Closed-loop system data of an attitude hold corrupted by measurement noise: (a) the input signal δ_e and (b) the attitude angle θ.

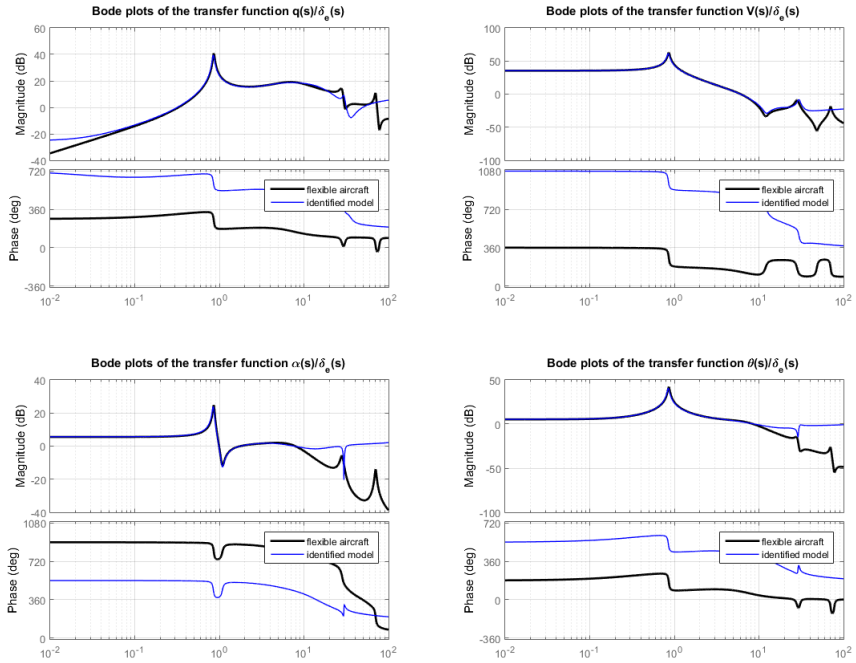

Figure 6 – Bode plots of the identified model from closed-loop system data corrupted by measurements noise.

CONCLUSIONS

This article presents a methodology in applying the subspace methods for flight vehicle system identification to an unmanned aerial system (UAS) with rigid-body dynamic coupled with wing bending modes. Preliminary results from simulated data of previous aircraft model operating in closed-loop suggest the approach can be applied to the aircraft system identification.

The identified model obtained from the DSR subspace algorithm can be referred as black-box model and one difficulty is to explicit the stability and control derivatives. Thus, the identified model have no physical meaning, but the preliminary numerical results suggest a good representative compared with others methods that perform an optimization problem, as the well-known OEM method widely discussed in [12].

Further work, the methodology presented in this work will be applied on closed-loop experimental data collected from flight campaigns with the UAS. The idea is to obtain a set of accuracy linear models for a required flight envelope that permits to perform a control-law minimizing the structural effects. Moreover, the identified model will be suitable for updating the parameters used for simulation and validation of the flexible aircraft model.

ACKNOWLEDGMENTS

The authors thanks the financial support for this work provided by CAPES (Coordenação de Aperfeiçoamento de Pessoa de Nível Superior).

REFERENCES

[1] Almeida F.A. and Silva, B.G.O., 2013, "Attenuation of aircraft flexible modes during maneuvering flight", AIAA Guidance, Navigation and Control.

[2] Bauer, D., 2001, "Order estimation for subspace methods" , Journal of Dynamic Systems, Measurement, and Control, Vol. 37, No. 10, pp. 1561–1573.

[3] Bronz, M. and Hattenberger, G., 2016, "Aerodynamic characterization of an off-the-shelf aircraft via flight test and numerical simulation", AIAA Flight Testing Conference.

[4] Bryson, A.E., 1994, "Control of Spacecraft and Aircraft".

[5] De Moor, B. and Overschee, P.V., 1996, "Subspace identification for linear sysyems: theory, implementations, applications.", Kluwer Academic Publichers.

[6] Diana, G. and Fiammenghi, G., 2012, "Wind tunnel tests and numerical approach for long span bridges: the Messina bridge", The Seventh International Colloquium on Bluff Body Aerodynamics and its Applications (BBAA7).

[7] Di Ruscio, D., 2009, "A Bootstrap Subspace Identification Method: comparing methods for closed loop subspace identification by Monte Carlo simulations", Journal of Modeling, Identification and Control, v. 30, n. 4, p. 203-222.

[8] Ewins, D. J., 1984, "Modal Testing: Theory and Practice", Published by Research Studies Ltd.

[9] Forssell, U., 1999, "Closed-loop identification: methods, theory, and applications", Pd.D in Electrical Engineering, Linköping University, p. 263.

[10] Huang, T., Yang, K., Cheng, R., Mu H. and Zhu, Y., 2016, "Closed-loop subspace identification of MIMO motion system with flexible structures for motion control", ASME 2016 INternational Mechanical Engeneering Congress and Exposition IMECE2016.

[11] Jammoussi, H., Franchek, M. and Grigoriadis, K., 2014, "A simulation study of the flight dynamics of elastic aircraft, results and analysis" , Vol. 136, Journal of Dynamic Systems, Measurement, and Control.

[12] Jategaonkar, R.V., 2006, "Flight vehicle system identification", Published by American Institute of Aeronautics and Astronautics, Vol. 216.

[13] Katayama, T., 2005, "Subspace Methods for System Identification: a realization approach", Kyoto: Springer.

[14] Klimmek, T., Ohme, P., Ciampa, P.D. and Handojo, V., 2016, "Aircraft loads - an important task from pre-design to loads flight testing", DLR, German Aerospace Center.

[15] Machado, R.C., 2013, "Métodos de subespaços para identificação de sistemas em malha fechada", Master's Thesis.

[16] Schmidt, D.K., 2013, "A non-linear simulink simulation of a large, flexible aircraft-FLEXSIM", Project supported by MUSYN, Inc., Minneapolis, MN.

[17] Schmidt, D.K., 2013, "Modern fligth dynamics", New York: Mc Graw-Hill.

[18] Silva,B.G.O. and Mönnich, W., 2012, "System identification of flexible aircraft in time domain", AIAA Atmospheric Flight Mechanics Conference.

[19] Silva, B.G.O., 2011, "Data gathering and preliminary results of the system identification of a flexible aircraft model", AIAA Atmospheric Flight Mechanics Conference.

[20] Stevens, B.L. and Lewis, F.L., 1992, "Aircraft Control and Simulation", Canada: John Wiley.

[21] Waszak, M.R. and Schmidt, D.K., 1988, "Flight Dynamics of aeroelastic Vehicles", J. Aircraft, Vol. 25, No. 6, pp. 563-571.

[22] Waszak, M.R, Davidson, J.B. and Schmidt, D.K., 1987, "A simulation study of the flight dynamics of elastic aircraft, results and analysis", Vol. 2, NASA Contractor Report 4102.

RESPONSIBILITY NOTICE

The author(s) is (are) the only responsible for the printed material included in this paper.